ATR Performance Prediction Using Attributed Scattering Features *

Hung-Chih Chiang and Randolph L. Moses

Department of Electrical Engineering, The Ohio State University

ABSTRACT

We present a method for estimating classification performance of a model-based synthetic aperture radar (SAR) automatic target recognition (ATR) system. Target classification is performed by comparing a feature vector extracted from a measured SAR image chip with a feature vector predicted from a hypothesized target class and pose. The feature vectors are matched using a Bayes likelihood metric that incorporates uncertainty in both the predicted and extracted feature vectors. We adopt an attributed scattering center model for the SAR features. The scattering attributes characterize frequency and angle dependence of each scattering center in correspondence the geometry of its physical scattering mechanism. We develop two Bayes matchers that incorporate two different solutions to the problem of correspondence between predicted and extracted scattering centers. We quantify classification performance with respect to the number of scattering center features. We also present classification results when the matchers assume incorrect feature uncertainty statistics.

Keywords: synthetic aperture radar, model-based target recognition, scattering centers, Bayes classification

1. INTRODUCTION

SAR target recognition is a challenging M-ary classification problem because of the high variation present in measured imagery. SAR backscatter returns of targets can change substantially with only slight differences in target pose (azimuth and elevation) or target articulation (position of a moving part on the target). As a result, each target class is a multimodal composite class with a very large number of dissimilar subclasses. If classification is attempted using template matching, the number of test templates becomes prohibitive in practical problems.

To address the dimensionality of the SAR ATR problem, the classification problem is subdivided into stages; a typical three-stage system[1] is shown in Figure 1. The stages employ successively more sophisticated data processing on successively fewer regions of the data and classification spaces. The first stage is a prescreener which performs initial detection of regions of interest (ROI) that may contain targets of interest. The indexer stage operates on regions of interest detected in the first stage. The indexer further reduces non-target false alarms, and estimates a candidate list of potential targets hypotheses along with a coarse pose estimate for each target hypotheses, usually using a coarsely tuned set of templates or features. The coarse estimation is designed to reduce the search space for the classifier stage. The classifier is the most computationally intensive process, and estimates the final target class.

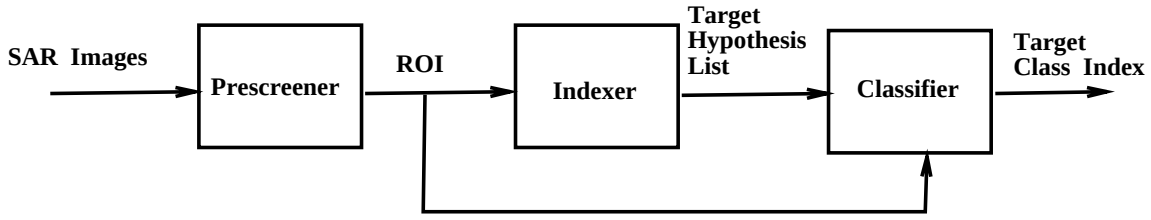

Figure 1. A typical SAR ATR system

To address the problem of a very large number of classes, some ATR systems have adopted a model-based approach. An example of such a model-based ATR system is the Moving and Stationary Target Acquisition and Recognition (MSTAR) ATR system.[2–4] In model-based methods, classification is performed by comparing a feature vector extracted from a measured SAR image chip with a feature vector predicted from a hypothesized target class

* This research was supported in part by DARPA and the US Air Force Research Laboratory under Grant F33615-979191020.

and pose. The feature vectors are compared using a Bayes likelihood match metric that incorporates uncertainty in both the predicted and extracted feature vectors. Generally, the predicted vector is computed on-line; the prediction engine can be thought of as a black box whose input is the hypothesized target class and pose and whose output is a predicted feature vector, along with feature uncertainty for the prediction. The predicted feature vector is then compared with the feature vector extracted from the SAR region of interest to determine if there is a match. The MSTAR classification output is computed by iteratively refining initial hypotheses (target and pose) generated at the output of the indexer. These features are matched using a Bayesian classifier which computes the likelihood of an extracted feature set given a predict hypothesis.[3]

In this paper we consider a model-based Bayesian matcher similar to the MSTAR matcher.[2–4] In our work, we consider an alternate set of features for SAR ATR. The feature set is based on an *attributed scattering center* model for target scattering.[5–7] In this model, the backscattered energy present in SAR imagery is modeled as a collection of scattering centers, each characterized by parameters that relate to the physical properties of the scattering mechanism. We develop a Bayesian matcher for the attributed scattering center features, and presents classification performance results using these features. The goal of performance estimation is to quantify the classification performance improvement realized by incorporating additional scattering attributes in a model-based SAR ATR system.

An outline of the paper is as follows. In Section 2 we present the attributed scattering center model that is used for classification. Section 3 presents the proposed Bayesian classifier. In Section 4 we present classification results using this scattering center model and classifier. Section 5 outlines conclusions and future research plans.

2. ATTRIBUTED SCATTERING CENTER MODEL

In this paper we employ a physically-based model for backscattered responses from objects measured at high frequencies.[6] The model approximates the scattering response by a sum of responses from individual scattering centers; each scattering center response is modeled using the dominant terms of monostatic scattering solutions from both Physical Optics and the Geometric Theory of Diffraction. The model incorporates both frequency and aspect dependence of scattering centers. Each scattering center is characterized by a set of parameters describing its location, amplitude, shape, and orientation angle. The model generalizes the common point scattering model[8,9] which assumes scattering centers are isolated points whose responses are identical to one another (except for amplitude), and are independent of frequency and angle. The attributed scattering center model provides a richer, physically relevant description of scattering behavior.

The attributed scattering center model parameterizes the total scattered field as a function of frequency f and aspect ϕ as a sum of p individual scattering center components:

$$E^s(f,\phi) = \sum_{k=1}^{p} E_k^s(f,\phi) \tag{1}$$

where each scattering center is modeled as

$$E_k^s(f,\phi) = A_k \left(j\frac{f}{f_c}\right)^{\alpha_k} \exp(-2\pi f \gamma_k \sin\phi)\mathrm{sinc}\left(\frac{2\pi f}{c} L_k \sin(\phi-\bar{\phi}_k)\right) \exp\left(j\frac{4\pi f}{c}(x_k\cos\phi + y_k\sin\phi)\right) \tag{2}$$

Here, (x_k, y_k) denote the scatterer location, A_k is its amplitude, α_k is its frequency dependence. Each scattering center is either localized or distributed; for localized scattering centers $L_k = \bar{\phi}_k = 0$ and γ_k characterizes the (mild) aspect dependence of the scattering center. For distributed scattering centers $\gamma_k = 0$, and scattering aspect dependence is described by the physical length L_k and orientation angle $\bar{\phi}_k$). The scattering model is thus described by a subset of the parameter set $(A_k, x_k, y_k, \alpha_k, \gamma_k, L_k, \bar{\phi}_k)$ for $k = 1, ..., p$.

The attributed scattering center model incorporates differences in scattering due to different object geometries. For example, trihedral (corner reflector) scattering is characterized by $\alpha = 1,\ L = 0$, dihedral by $\alpha = 1,\ L > 0$, and spherical surfaces by $\alpha = 0,\ L = 0$. The point scattering model is a degenerate case of this model with $\gamma_k = L_k = \bar{\phi}_k = \alpha_k = 0$. The point scattering model contains no aspect and frequency dependence description of scatterers, and one cannot discriminate between different physical scattering mechanisms from its model parameters.

Algorithms for estimating the scattering model parameters from measured SAR imagery are presented in.[6,7,10,11] Uncertainty of the scattering features has been considered in.[6,11] The Cramér-Rao bound for the features is presented

in,[6] and initial comparisons of estimation algorithm performance to the CRB are presented in.[6,10,11] Refinement of estimation algorithms and estimation uncertainty remain topics of ongoing research.

2.1. Feature Statistics

In order to match an extracted feature vector to a predicted one, we need a statistical model of features. In model-based ATR, there is uncertainty in both extracted features and predicted features. In this section we develop a model for feature uncertainty for both extracted and predicted features. The feature uncertainty model is based partly on available theoretical and experimental performance results, and is partly motivated by computational simplicity of the Bayesian matcher.

We denote a predicted feature vector for a given target hypothesis H_i (where H_i indicates both target class and target pose) as a random vector X, and the corresponding extracted feature vector as Y. We see that

$$X = [X_1, X_2, \ldots, X_{N_x}]^T, \qquad Y = [Y_1, Y_2, \ldots, Y_{N_y}]^T \tag{3}$$

where N_x, N_y are the number of predicted and extracted scattering centers, respectively. Each X_i and Y_j is a vector of scattering attributes given by a subset of $(A_k, x_k, y_k, \alpha_k, \gamma_k, L_k, \bar{\phi}_k)$.

In order to match feature vectors X and Y, we need a model for the probability density functions $f(X|H)$ and $f(Y|X,H)$. We assume the X_i are conditionally independent given H, and that Y_i are conditionally independent given H and X. The independence of the X_i is based on the fact that prediction errors of separate scattering centers would be due to variations in components on the target that make up that scattering center, and these variations are generally not closely related. The independence of the Y_i is supported by the near block diagonality of the Cramér-Rao bound matrix for well-separated scattering centers.[6] We further assume that the individual parameters that make up each X_i and Y_j are independent. Again, the CRB matrix is diagonally dominant, supporting this assumption. In addition, since little empirical information exists to either support or contradict an independence assumption, and since the independence assumption simplifies the Bayes matcher significantly, we are inclined to adopt the independence assumption until sufficiently compelling evidence becomes available to suggest otherwise.

The Bayes match metric developed below uses a subset of the available attributed scattering features that are expected to provide the best improvement in class separability. We do not match the γ_k and $\bar{\phi}_k$ parameters because they are expected to have high uncertainty in practical systems. In addition, we quantize the information in the L_k feature to one bit; that is we assume the the predicted and extracted L_k feature is either that $L_k = 0$ or $L_k > 0$.

For prediction we assume the following probabilistic feature uncertainty statistics. For the downrange and cross-range location parameters (x_k and y_k), we assume the prediction uncertainty is Gaussian with zero mean and known standard deviation. Similarly, we assume a Gaussian uncertainty for α_k. The α_k uncertainty assumption is conservative, since α_k is directly related to curvatures of the surfaces on the target that make up the scattering center, and these should be known with almost no uncertainty. We assume L_k is predictable with no uncertainty. Finally, we assume that the scattering amplitude is log normal distributed to model the high degree of uncertainty in predicting scattering amplitude.

Some extracted features correspond to a scattering centers that are predicted for the target, and some are due to clutter peaks and do not correspond to predicted features. For extracted scattering centers that correspond to predicted features, we assume the same location, frequency dependence (α_k), and amplitude uncertainty model as we do for predict uncertainty, but with different standard deviations. We assume nonzero uncertainty in the extracted L_k parameter, which can be specified as a 2×2 confusion matrix.

In addition, extracted scattering features may arise from clutter peaks. We assume a uniform two-dimensional Poisson model for clutter peak detection, with an average of λ clutter peaks per pixel in the image. The location of clutter peaks are uniformly distributed on the target chip. We assume the remaining extracted clutter attributes have the same statistical model as target scattering attributes, but with different parameters (different standard deviations, for example).

3. BAYESIAN MATCHERS

In this section we present the Bayes match function used in our analysis. From a given region of interest on the SAR image, we assume the indexer generates an output list of candidate target classes and pose estimates. Using the assumptions for feature priors in Section 2,

We compute the likelihoods of the extracted feature vector given the hypotheses from the indexer. We can also compute the posterior probabilities of the hypotheses given the extracted feature. Then we apply either the maximum likelihood or maximum a posteriori probability decision rule for classification.

3.1. Feature Correspondences

Computing the Bayes likelihood requires that we form a correspondence between extracted and predicted features. An extracted feature vector is not ordered with respect to the corresponding predict feature vector. The correspondence must also account for extracted scattering centers Y_j that are not in the predicted vector (extraction false alarms) as well as predicted scattering centers X_i that are not extracted (missed extraction scattering centers). We consider two correspondence mappings below, adapted from Ettinger, *et. al.*[3] These two correspondence mapping lead to two different formations of the match likelihood functions. Let , denote a correspondence map. Define , $_j = 0$ if y_j is mapped from clutter and , $_j = i$ if y_j is mapped from x_i.[3]

Figure 2 shows a many-to-many correspondence map between a set of predicted scatterers and extracted scatterers. Each extracted scattering center is mapped to each predicted scattering center or clutter with some probability. Let $P_i(H)$ denote the probability of detecting the ith predicted scattering center under hypothesis H and let $|A|$ represent the image unambiguous range. Following Ettinger, *et. al.*,[3] we select

$$B = \frac{\lambda |A|}{\lambda |A| + \sum_k P_k(H)} \tag{4}$$

as the probability that the extracted scattering center comes from clutter, and

$$D_i(H) = (1 - B) \frac{P_i(H)}{\sum_k P_k(H)} \tag{5}$$

as the probability that the extracted scattering center comes from the ith predicted scattering center.

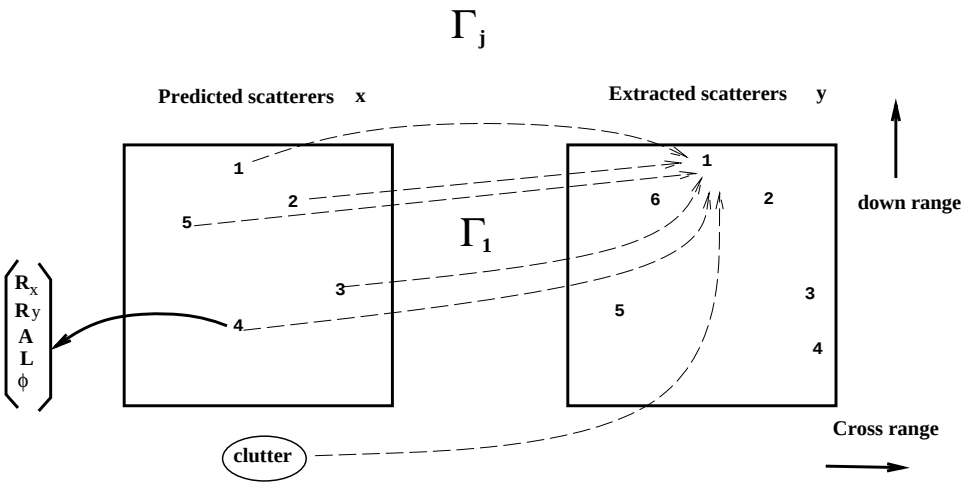

Figure 2. A many-to-many correspondence map between predicted scatterers and extracted scatterers

Figure 3 shows a one-to-one correspondence map. Each extracted scattering center is mapped from either one of the predicted scattering center or clutter.

3.2. Likelihood of a Single Scatterer

For a given extracted feature vector Y, we treat the feature vector for the independent scattering centers separately. Since we assume scattering center features are conditionally independent given a hypothesis, the likelihood of an extracted scattering center given a hypothesis H is the product of the likelihoods of its individual features given the hypothesis:

$$f(y_j|H) = \prod_\theta f(y_{j\theta}|H), \tag{6}$$

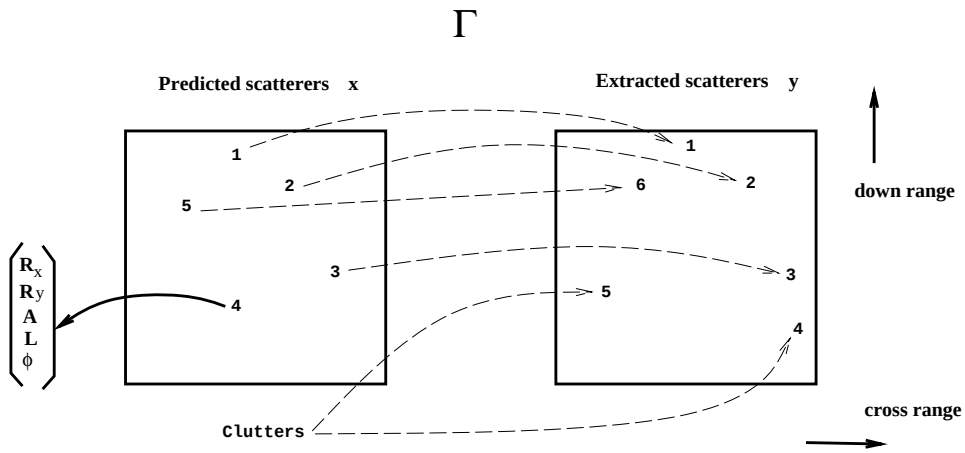

Figure 3. A one-to-one correspondence map between predicted scatterers and extracted scatterers

where θ denotes the feature parameter. A feature vector Y_j may arise from a target scattering center or may be a clutter peak. If Y_j results from clutter, its likelihood is governed by a clutter density. If Y_j is mapped from a predicted scatterer X_i, and if the feature has a Gaussian distribution (which is the case for the location parameters, the log amplitude, or the simplified type α), the likelihood is also Gaussian[12]:

$$f(y_{j\theta}|,\ _j = i, H) \ = \ \frac{1}{\sqrt{2\pi\sigma^2_{ij\theta}}} \exp\{(y_{j\theta} - x_{i\theta})^2/2\sigma^2_{ij\theta}\}. \tag{7}$$

Because of the independence assumption, the likelihood variance is the sum of the extraction uncertainty variance and prediction uncertainty variance. A discrete random variable feature $y_{j\theta} \in Y_j$ (such as the discrete length statistic) has likelihood given by a weighted sum of conditional mass functions

$$P(y_{j\theta}|,\ _j = i, H) \ = \ \sum_{\bar{x}_{i\theta}} P(y_{j\theta}|\bar{x}_{i\theta}, H) \ \cdot \ P(\bar{x}_{i\theta}|H) \ = \ \sum_{\bar{x}_{i\theta}} P(y_{j\theta}|\bar{x}_{i\theta}) \ \cdot \ P(\bar{x}_{i\theta}|x_{i\theta}). \tag{8}$$

3.3. Feature Likelihood Function

The maximum likelihood matcher requires the computation of the likelihood $f(y|H)$ for a many-to-many map, or $f(y,,\ |H)$ for a one-to-one map.

For the many-to-many map, we have

$$f(y|H) \ = \ \prod_j \ f(y_j|H) \ = \ \prod_j \ \left[B \ f_c(y_j) \ + \ \sum_i \ D_i(H) f(y_j|,\ _j = i, H) \right] \tag{9}$$

We use the independent scattering center assumption in the first equality, and the many-to-many mapping structure (4)–(5) in the second equality.

For the one-to-one map we adopt the following likelihood expression[13]

$$f(y,,\ |H) \ = \ e^{-\lambda|A|} \frac{(\lambda|A|)^f}{m!} \left(\prod_{\{j:,\ _j=0\}} f_c(y_j) \right) \left(\prod_{\{j:,\ _j\neq 0\}} P_{,\ _j} \ f(y_j|,\ _j = i, H) \right) \left(\prod_{\{k:,\ _j\neq k, \forall j\}} (1 - P_k(H)) \right), \tag{10}$$

where f is the number of clutter scattering centers given by the correspondence map , , and m is the total number of extracted scattering centers. The $f(y,,\ |H)$ expression includes the number and permutations of clutter scattering centers, density of extracted scattering centers given a correspondence map, and missing predicted scattering centers.

3.4. Maximum likelihood matchers

Let T denote the target class decision by the classifier. The maximum likelihood (ML) match scores given by

$$T = \text{ind} \max_{H_i} f(y|H_i), \qquad \text{many-to-many map} \tag{11}$$

$$T = \text{ind} \max_{,\,,H_i} f(y,,\,|H_i), \qquad \text{one-to-one map} \tag{12}$$

The ML matcher for the one-to-one map requires the search of all possible correspondences , . This is computationally more expensive than the ML matcher for the many-to-many map.

	y_1	$\cdots$	y_n
x_1	$D_1(H)f(y_1\|,\,_1 = 1, H)$	$\cdots$	$D_1(H)f(y_n\|,\,_n = 1, H)$
$\vdots$	$\vdots$	$\ddots$	$\vdots$
x_m	$D_m(H)f(y_1\|,\,_1 = m, H)$	$\cdots$	$D_m(H)f(y_n\|,\,_n = m, H)$
FA_1	$Bf_c(y_1)$		0
$\ddots$		$\ddots$	
FA_n	0		$Bf_c(y_n)$

Table 1. The likelihood matrix for the many-to-many matcher in equation (9). FA_k denotes a false alarm corresponding to the kth extract feature.

	y_1	$\cdots$	y_n	MI_1	$\cdots$	MI_m
x_1	$-\log P_1(H)f(y_1\|,\,_1 = 1, H)$	$\cdots$	$-\log P_1(H)f(y_n\|,\,_n = 1, H)$	$-\log(1 - P_1(H))$		∞
$\vdots$	$\vdots$	$\ddots$	$\vdots$		$\ddots$	
x_m	$-\log P_m(H)f(y_1\|,\,_1 = m, H)$	$\cdots$	$-\log P_m(H)f(y_n\|,\,_n = m, H)$	∞		$-\log(1 - P_m(H))$
FA_1	$-\log \lambda\|A\|f_c(y_1)$		∞	0	$\cdots$	0
$\vdots$		$\ddots$		$\vdots$	$\ddots$	$\vdots$
FA_n	∞		$-\log \lambda\|A\|f_c(y_n)$	0	$\cdots$	0

Table 2. The cost matrix for the one-to-one matcher in equation (10). FA_k denotes a false alarm corresponding to the kth extract feature. MI_k denotes that the kth predict feature was missed by the extracter.

Table 1 shows the likelihood matrix for the many-to-many matcher in equation (9) and Table 2 shows the cost matrix for the one-to-one matcher in equation (10). Each element in the cost matrix is the negative of the logarithm of a corresponding weighted likelihood. For the many-to-many matcher in equation (9) the likelihood scores of the jth column in Table 1 are added to obtain the likelihood for the jth extracted scattering center, then the summed scores are multiplied together to form the likelihood for the extracted feature vector y given hypothesis H. For the one-to-one matcher in equation (10), only one cost entry for each column in Table 2 is selected as the cost for the jth extracted scattering center. All such selected cost entries of columns must have different row indices. The matcher searches all possible correspondences to find the lowest cost. We use the Hungarian algorithm adapted from combinatorial optimization[14] to effectiently search for the best correspondence.

The one-to-one and many-to-many ML match scores can be related as follows. Let y be an extracted feature vector of N_y scattering centers. Without loss of generality suppose $y_j, j = 1, ..., N_t$ correspond to $x_i, i = 1, ..., N_t$, respectively, $y_i, i = N_t+1, ..., N_y$ correspond to clutter, and $x_i, i = N_t+1, ..., N_x$ are missed target predicted scattering center. Assuming the estimation error is small enough such that

$$f(y_j|,\,_j = j, H) \;\gg\; f(y_j|,\,_j = k, H),\ \forall j \in \{1, ..., N_t\},\ k \neq j, \tag{13}$$

and

$$f_c(y_j) \;\gg\; f(y_j|,\,_j = k, H),\ \forall j \in \{N_t + 1, ..., N_y\},\ \forall k \in \{1, ..., N_x\} \tag{14}$$

and also assuimng the correct correspondence map is adopted, then the one-to-one likelihood $f(y,,|H)$ in equation (10) can be approximated as

$$f_1(y|H) \approx e^{-\lambda|A|}\frac{(\lambda|A|)^{N_y-N_t}}{N_y!}\left(\prod_{k=N_t+1}^{N_y} f_c(y_k)\right)\left(\prod_{k=1}^{N_t} P_k(H)\ f(y_k|,_k=k,H)\right)\left(\prod_{k=N_t+1}^{N_x}(1-P_k(H))\right), \quad (15)$$

and the many-to-many likelihood $f(y|H)$ in equation (9) can be approximated as

$$f_m(y|H) \approx B^{N_y-N_t}\left(\prod_{N_t+1}^{N_y} f_c(y_k)\right)\left(\frac{1-B}{\sum_{j=1}^{N_x} P_j(H)}\right)^{N_t}\left(\prod_{k=1}^{N_t} P_k(H)\ f(y_k|,_k=k,H)\right). \quad (16)$$

The ratio of $f_1(y|H)$ to $f_m(y|H)$ is

$$\frac{f_1(y|H)}{f_m(y|H)} \approx \frac{1}{N_y!}\ e^{-\lambda|A|}\ B^{-N_y}\ (\lambda|A|)^{N_y}\sum_{k=N_t+1}^{N_x}(1-P_k(H)). \quad (17)$$

Equation (17) is independent of y. The difference between these two matchers thus depends on N_y, N_x, N_t and $P_k(H), k=1,...,N_x$ in (17). The simulations in Section 4 compare their performance and computation time empirically.

3.5. Maximum A Posteriori Probability Matching

Let $P(H_i)$ denote the priors of hypotheses from Index. $\sum_i\ P(H_i)=1$. By Bayes rule we have

$$f(H_i|y) = \frac{f(y|H_i)P(H_i)}{\sum_k\ f(y|H_k)P(H_k)} \quad (18)$$

The maximum *a posteriori* probability matcher for a many-to-many map is

$$T = \text{ind}\max_{H_i}\ f(H_i|y) \quad (19)$$

For one-to-one map, we can use

$$T = \text{ind}\max_{H_i}\ \frac{(max,\ f(y,,|H_i))P(H_i)}{\sum_k\ (max,\ f(y,,|H_k))P(H_k)} \quad (20)$$

While a maximum *a posteriori* probability match gives more insight on how to set the threshold value for false alarm rejection than does a maximum likelihood matcher. On the other hand the maximum *a posteriori* computation requires additional prior information from the indexer.

4. PERFORMANCE EVALUATION

In this section we estimate the classification performance results from the Bayesian matcher, and compare classification performance in a variety of scenarios. We establish a simulation using feature vector means based on measured SAR imagery, coupled with an assumed feature perturbation model. The perturbation model is in some cases matched to the classifier, and in some cases mismatched. We compare performance when using two features (location, amplitude) to performance when using four features (location, amplitude, α, L). We also compare classification performance with respect to the number of scattering center features in one scenario.

4.1. Data and Experimental Procedure

Our simulations are based on features extracted from ten targets in the MSTAR Public Targets dataset. These are X-band image chips with 128x128 pixels at 0.3m×0.3m resolution, and at 17 degree depression angle. There are a total of 2747 images; for each of the ten targets approximately 270 images are available covering 360 degrees in azimuth. Target classes 1 to 10 are the 2S1, BMP2, BRDM2, BTR70, BTR60, D7, T62, T72, ZIL131, and ZSU_23_4, respectively.

Peak features (down/cross range locations and magnitude of peak amplitudes) are extracted from each image chip using a peak extraction routine which essentially finds local maxima in the SAR image. The nominal values of the type attribute are generated using a Gaussian random variable with mean 0.5 and standard deviation 0.5. The nominal values of the length attribute are generated using a Bernoulli random variable with a probability of 0.1 that $L > 0$. These form the 2747 class mean vectors for the 10 composite target classes.

We generate both predicted feature vectors and the extracted feature vectors by perturbing the above class mean vectors. The noise perturbations we use on the feature attribute means are:

- Predicted features:
  down-range and cross-range locations: $N(0,1)$ image pixel
  amplitude: $\log_{10}(|A|)$ is $N(0,0.5)$
  type: α is $N(0,0.5)$
  length: no uncertainty, so the L confusion matrix is $\begin{bmatrix} 1 & 0 \\ 0 & 1 \end{bmatrix}$
- Extracted features:
  down-range and cross-range locations: $N(0,1)$ image pixel
  amplitude: $log_{10}(|A|)$ is $N(0,0.5)$
  type: α is $N(0,0.5)$
  length: $P(\text{error}) = 0.2$, so the L confusion matrix is $\begin{bmatrix} 0.8 & 0.2 \\ 0.2 & 0.8 \end{bmatrix}$
- Clutter statistics:
  locations: 2D Poisson with a rate 3 clutter peaks per image chip
  amplitude: $\log_{10}(|A|)$ is $N(\mu,0.5)$, with μ= logarithm of the median amplitude of target scattering centers.
  Clutter type: α is $N(0.5,1)$
  Clutter length: L is Bernoulli with $P(L > 0) = 0.1$ or 0.3.

We emulate the prescreener and indexer as follows. For each of the 2747 target image chips, we find the 5 image chips in each of the 10 target classes that have the highest correlation with it. The targets and poses (pose is in this case azimuth angle) corresponding to these 50 image chips form the initial hypothesis list that is provided to the Bayes classifier.

Classification performance is measured as follows. For each of the 2747 test feature vectors, we generate 50 hypotheses from the indexer, and generate 10 predicted scattering centers for each hypotheses by randomly perturbing the class means as described above. We similarly generate 10 extracted scattering centers from the hypothesis class mean vector. The extract feature vectors assume each scattering center has a probability of detection that ranges from $P_d = 0.5$ to 0.9 depending on the experiment; thus, not all scattering centers are present in the extracted feature vector. We also add clutter scattering centers to the extract feature vector. We then compute the one-to-one likelihood function in equation (10) and the many-to-many likelihood function in equation (9) for the extracted scattering center given each hypothesis, and choose the one of the 50 hypotheses with the highest likelihood score. This gives a total of 27,470 classifications from 27,470×50 match scores.

Figure 4 shows an example of the SAR image data we used. The circles in Figure 4 indicate the scattering center locations.

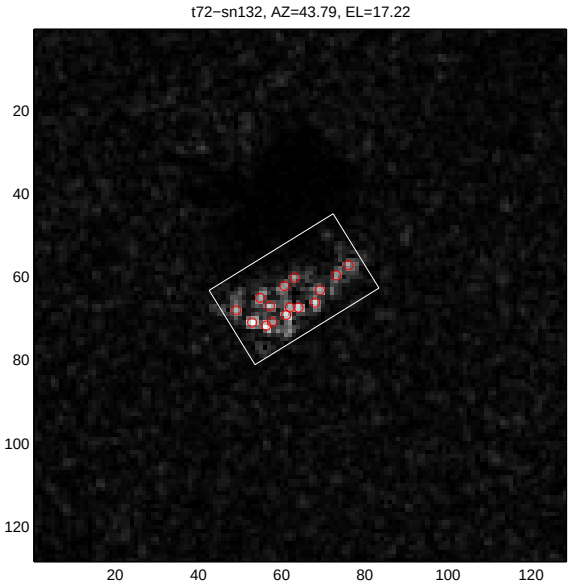

Figure 4. An example of the SAR image data used for simulation studies.

4.2. Baseline Performance Results

As a baseline experiment we considerd classification performance for both the one-to-one and many-to-many classifier using a scattering center detection probabilities of of 0.5, 0.7, and 0.9. We considered two cases for the feature vector, one using only location and amplitude features of scattering centers (the "two attributes" case) and one using location, amplitude, frequency dependence (α), and length (the "four attributes" case). Table 3 is a typical confusion matrix result from the test. We see that classification errors for all targets are fairly evenly spread over the other targets. This result is typical in the other experiments considered. We summarize the confusion matrix results in this and all other experiments by an average probability of correct classification for all 27,470 matches, as shown in Figure 5.

One-to-One Map, Four attributes with $P_d = 0.5$											
C4	T1	T2	T3	T4	T5	T6	T7	T8	T9	T10	Total
T1	2872	13	9	23	9	6	19	12	15	12	2990
T2	18	2233	7	11	10	7	8	11	14	11	2330
T3	11	13	2852	17	16	11	17	14	9	20	2980
T4	12	15	9	2255	7	5	4	6	11	6	2330
T5	14	8	4	11	2485	6	6	9	6	11	2560
T6	11	12	13	10	14	2874	14	13	11	18	2990
T7	16	13	19	13	8	21	2859	13	13	15	2990
T8	17	14	8	6	8	3	9	2235	9	11	2320
T9	16	11	16	11	11	9	12	8	2882	14	2990
T10	13	18	11	16	15	14	10	12	9	2872	2990

Table 3. Confusion matrix for one-to-one classification experiment using four scattering attributes. The overall correct classification rate is 96.17%.

From Figure 5 we see that additional type and length attributes reduces classification errors by about a factor of two. We also find that the classification performance using a many-to-many matcher is only slightly lower that the classification performance using a one-to-one matcher in this scenario. The one-to-one matcher requires the search for the best correspondence which introduces more computational complexity than the many-to-many matcher which only averages the likelihood scores pointwise. Table 4 shows the total time to compute likelihood scores for 500 pairs of (predict,extract) feature vectors in this experiment.

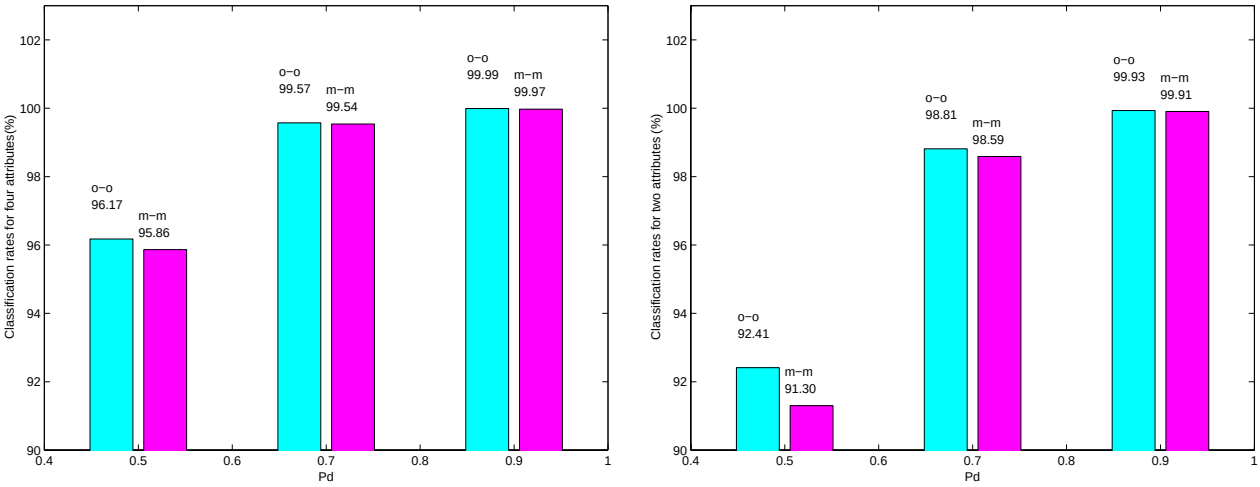

Figure 5. Classification performance using four and two attributes

	Pd=0.5	Pd=0.7	Pd=0.9
2 Attributes One-to-One	33.6	38.4	47.3
4 Attributes One-to-One	47.4	61.1	69.1
2 Attributes Many-to-Many	9.5	11.4	13.4
4 Attributes Many-to-Many	24.8	30.6	36.3

Table 4. the total CPU time (sec) to compute likelihood scores for 500 pairs of (predict,extract) feature vectors

4.3. Match Statistic Modeling Errors

In this experiment we generate predict and extract feature vectors whose feature uncertainty differs from the uncertainty assumed by the Bayes match. The uncertainty errors considered are in the scattering center location standard deviations. We perform a classification experiment assuming an actual location standard deviation of 2 pixels for both the predicter and extracter. In the Bayes matcher, we assume a location standard deviation of 1 pixel and 3 pixels. All the other feature uncertainties are as before, and are correct in the matcher.

Figure 6 shows the classification performance using one-to-one matcher, where Matcher 1 uses the correct standard deviation, Matcher 2 assumes the standard deviation is 1 pixel, and Matcher 3 assumes the standard deviation is 3 pixels. We see that using the incorrect location uncertainty does not substantially affect classification performance. We see that underestestimating location uncertainty results in lower degradation of classification performance than does overestimating uncertainty for this example. Also, the performance loss is smaller when four scattering attributes are used.

4.4. Classificaton Performance versus Number of Scattering Attributes

In this experiment we compare classification performance using one attribute (location), two attributes (location and amplitude), three attributes (location, amplitude, and α or location, amplitude, and length), and four attributes (location, amplitude, α, and length). We use ten scattering centers with the same perementers as in Section 4.2, but we fix $P_d = 0.5$ and $P(y_{jL} = 0) = 0.7$. Both one-to-one and many-to-many matchers are employed.

The results are shown in Figure 7. We see that the classification rates increase from 87.60% (86.15%) to 96.20% (96.19%) for the one-to-one (many-to-many) matcher as we increase the number of scattering attributes from one to four. The results also show that the computationally inexpensive many-to-many matcher gives nearly the same performance as the one-to-one matcher for this case.

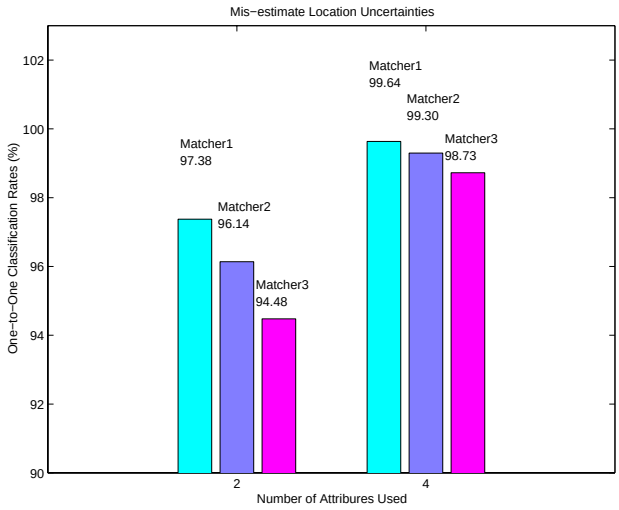

Figure 6. Classification performance for a one-to-one matcher using errorous location uncertainties in the Bayes matcher. Matcher 1: correct uncertainty used; Matcher 2: location uncertainty assumed is 0.5 times true uncertainty; Matcher 3: location uncertainty assumed is 2 times true uncertainty.

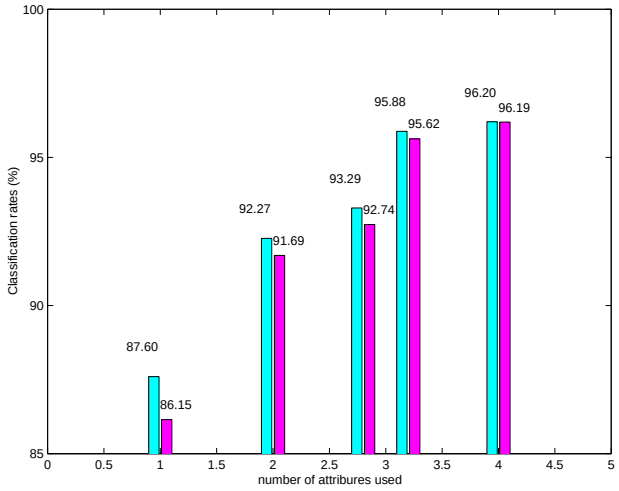

Figure 7. Classification performance versus number of scattering attributes used. The attributes used are: 1: location; 2: location and amplitude; 3: location, amplitude, and α (left), or location, amplitude, and length (right); 4: location, amplitude, α, and length. Classification results are shown for the one-to-one (light gray) and many-to-many (dark gray) matchers.

5. CONCLUSIONS

We have developed a method for estimating classification performanc for a model-based ATR system that employs attributed scattering center features. The classifier is based on a Bayes match between vector of extracted scattering features and a vector of predicted features. Uncertainty in both extracted and predicted features are included in the match metric. The match requires estimating the correspondence between extracted and predicted features, and the correspondence must take into account both false alarm and missed scattering centers in the extracted feature vector. We considered two match correspondence strategies, a one-to-one match and a computationally simpler many-to-many match.

We presented classification performance predictions based on scattering centers extracted from measured SAR imagery of ten targets. A total of 2747 images were used to obtain classificaton performance results. The results indicate that additional scattering attributes reduce classification errors by about a factor of two for the feature uncertainty models we considered. In addition, we found that the the many-to-many matcher performs only slightly worse than the one-to-one matcher, but is computationally much less expensive than the one-to-one matcher.

The actual classification performance will be highly dependent on the actual feature uncertainty encountered in practice. Our uncertainty model attempts to provide a reasonable estimate of anticipated feature uncertainty, but more work is needed to understand the nature of both prediction and extraction uncertainties of scattering attributes. Studies on feature uncertainty bounds and on feature uncertainties of extraction algorithms show that most features have lower uncertainty as SAR resolution increases, so the relative benefit in classification performance improvement realized by additional scattering attributes may change substantially as resolution changes. This is a topic of current research by the authors.

ACKNOWLEDGMENTS

The authors are grateful to Dr. William Irving at Alphatech, Inc. for his many technical suggestions and for providing Matlab code for feature correspondence. The author also wish to thank Dr. Warren Smith at SAIC Tuscon for a Matlab implementation of the MSTAR peak extractor.

REFERENCES

1. L. M. Novak, G. J. Owirka, and C. M. Netishen, "Radar Target Identification Using Spatial Matched Filters," *Pattern Recognition* **27**(4), pp. 607–617, 1994.
2. E. R. Keydel and S. W. Lee, "Signature Prediction For Model-Based Automatic Target Recognition," *SPIE* **2757**, pp. 306–317, Apr. 1996.
3. G. J. Ettinger, G. A. Klanderman, W. M. Wells, and W. E. L. Grimson, "A Probabilistic Optimization Approach To SAR Feature Matching," *SPIE* **2757**, pp. 318–329, Apr. 1996.
4. J. Wissinger, R. Washburn, D. Morgan, C. Chong, N. Friedland, A. Nowicki, and R. Fung, "Search Algorithms For Model-Based SAR ATR," *SPIE* **2757**, pp. 279–293, Apr. 1996.
5. L. C. Potter and R. L. Moses, "Attributed Scattering Centers for SAR ATR," *IEEE Trans. Image Processing* **6**, pp. 79–91, Jan. 1997.
6. M. Gerry, *Two-dimensional Inverse Scattering Based on the GTD Model*. PhD thesis, The Ohio State University, Columbus, OH, 1997.
7. R. L. Moses, L. C. Potter, H.-C. Chiang, M. Koets, and A. Sabharwal, "A Parametric Attributed Scattering Center Model for SAR Automatic Target Recognition," *Proceedings of the 1998 Image Understanding Workshop*, pp. 849–860, Nov. 1998.
8. M.-W. Tu, I. Gupta, and E. Walton, "Application of Maximum Likelihood Estimation to Radar Imaging," *IEEE Trans. Antennas and Propgation* **45**(1), pp. 20–27, 1997.
9. J. J. Sacchini, W. M. Steedly, and R. L. Moses, "Two-Dimensional Prony Modeling and Parameter Estimation," *IEEE Trans. on Signal Processing* **41**, pp. 3127–3137, Nov. 1993.
10. M. A. Koets and R. L. Moses, "Image Domain Feature Extraction from Synthetic Aperture Imagery," in *ICASSP*, (Phoenix, AZ), Mar. 1999.
11. M. Koets, "Automated Algorithms for Extraction of Physically Relevant Features from Synthetic Aperture Radar Imagery," Master's thesis, The Ohio State University, Columbus, OH, 1998.
12. H.-C. Chiang, "Bayesian Matching for Attributed Scattering Centers," Ph.D. Research Proposal, The Ohio State University, 1998.
13. W. W. Irving, "personal communication," July 1998.
14. C. H. Papadimitriou and K. Steiglitz, *Combinatorial Optimization Algorithm and Complexity*, Prentice-Hall, Englewood Cliffs, New Jersey, 1982.